Application of Au@SiO₂ Plasmonic Nanoparticles at Interface of TiO₂ Mesoporous Layers in Perovskite Solar Cells

Naemeh Aeineh[a], Nafiseh Sharifi[b,*], and Abbas Behjat[a,c]

[a]Atomic and Molecular Group, Faculty of Physics, Yazd University, Yazd, Iran
[b]Physics Department, University of Kashan, Kashan, Iran
[c]Photonics Research Group, Yazd University, Yazd, Iran
[*]Corresponding author: sharifi@kashanu.ac.ir

ABSTRACT— To investigate the plasmonic effect in perovskite solar cells, the effect of depositing Au@SiO₂ nanoparticles on the top and the bottom of mesoporous TiO₂ layers was studied. First, Au@SiO₂ nanoparticles were synthesized. The particles were then deposited at the different interfaces of mesoporous TiO₂ layers. Although the two structures show approximately similar optical absorption, only cells with Au@SiO₂ nanoparticles deposited at the bottom of the mesoporous TiO₂ layers demonstrated an improved photocurrent performance compared to the reference cells. This structure shows a short-circuit current density (JSC) of 20.7 mA/cm² and open circuit voltage of 1081 mV. This enhancement may be attributed either to the interface surface engineering or plasmonic resonance of Au@SiO₂ nanoparticles depends to the NPs size and position.

KEYWORDS: Photovoltaic, Perovskite solar cells, Au@SiO₂ nanoparticles, Plasmonic nanoparticles, Core-shell.

I. INTRODUCTION

In recent years, organic−inorganic perovskites materials have been widely investigated as light harvester in solar cells. They have superior properties including direct band gap, large absorption coefficients, and high carrier mobility which enabling us to be used as a light harvester in a solar cell [1]. The Maximum power conversion efficiency (PCE) of perovskite based solar cells is reported from 3.8% in 2009 [2] to over 22.1% in recent years [3]. To increase efficiency, it is necessary to extend light absorption spectrum, by means of applying noble metal nanoparticles (NPs), increase the active layer thickness, inserting scattering layers, and back reflectors layers or other light trapping elements [4]–[6]. The addition of noble metal gold (Au), silver (Ag) and aluminum (Al) NPs in the hole transport layer (HTL) of planar inverted perovskite solar cells showed that electron extraction and in turn device efficiency are enhanced [7]. An effective method has also been investigated in perovskite devices to achieve efficient performance by combinational use of Au NPs insulating by MgO [8]. Also, different amount of Au@SiO₂ core–shell NPs have been deposited as a modifier of the mp-TiO₂ layer in perovskite solar cells, and the enhanced in device performance and increase in light absorption are reported [9].

Au and Ag are the most commonly used plasmonic materials, and they have also been combined with oxide cores or shells [10]–[12]. The maximum PCE of 16.3% was reported in perovskite solar cell having plasmonic structure [11]. More recently, the role of NPs in perovskite solar cells has been investigated theoretically [13],[14]. They showed Au@SiO₂ core-shell NPs provide optical absorption enhancement in perovskite solar cells, where the perovskite material itself has relatively poor absorption. Also, they showed

Au@SiO$_2$ NPs with a SiO$_2$ shell thickness of ~1 nm provided greater absorption enhancement than the NPs with thicker shells [13]. In previous work, our group studied the plasmonic effects of Ag NPs (Ag NPs without shell) on the photovoltaic characteristics of mesoporous heterojunction HTL-free perovskite solar cells [15]. Most recently we have studied and reported the dramatic role of Au@SiO$_2$ NPs in the perovskite solar cells interfaces, where, the use of reduced quantities of highly stable inorganic compounds modified the PSC interface instead of the extensively used organic compounds [16].
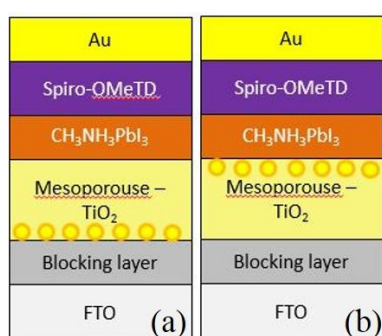
Fig. 1. Schematic of perovskite solar cell structures showing Au@SiO$_2$ NPs (a) the bottom and (b) on the top of the mp-TiO$_2$ layers.

In this study, we studied two methods of photocurrent enhancement on perovskite solar cells in which Au@SiO$_2$ NPs were deposited on the bottom and the top of a mesoporous TiO$_2$ (mp-TiO$_2$) as an interface layer (Fig.1). It is shown that the both structures by using Au@SiO$_2$ NPs increases the short-circuit current_density of the fabricated cell, while enhancement by using Au@SiO$_2$ NPs was deposited on the bottom of mp-TiO$_2$ is more significant.

II. EXPERIMENTAL PROCEDURE

A. *Cell Fabrication*

NP Synthesis. An Au sol is prepared based on Turkevich procedures [17]. Briefly, 250 mL of HAuCl$_4$ solution (1 mM), 25 mL of 1% sodium citrate solution was added, with boiling and vigorous stirring. After 10 min, the mixture produces a stable, deep-red dispersion of Au particles. An average diameter of Au was around 11 nm.

For Au@SiO$_2$ core/shell NPs Synthesis, Au@SiO$_2$ core-shell NPs were prepared according to the synthetic protocol of Liz-Marzan [18]. Briefly, 2.5 mL freshly prepared 1 mM aqueous solution of (3-aminopropyl) trimethoxysilane (APS) was added to 500 mL of the Au solution under vigorous magnetic stirring. The mixture was stirred for 15 min to ensure complete the amine groups with the Au surface. Then the 20 mL active silica with lowering the pH of a 0.54 wt % sodium silicate solution was added to 500 mL of the surface-modified Au solution under vigorous magnetic stirring. After stirring for 24 h, the NPs were collected by centrifugation at 15000 rpm for 1 h, washed three times with deionized water, and finally re-dispersed in ethanol. The thickness of silica shell was about 1.4 nm with an absorption peak at ~550 nm in water, as shown in Fig. 2.
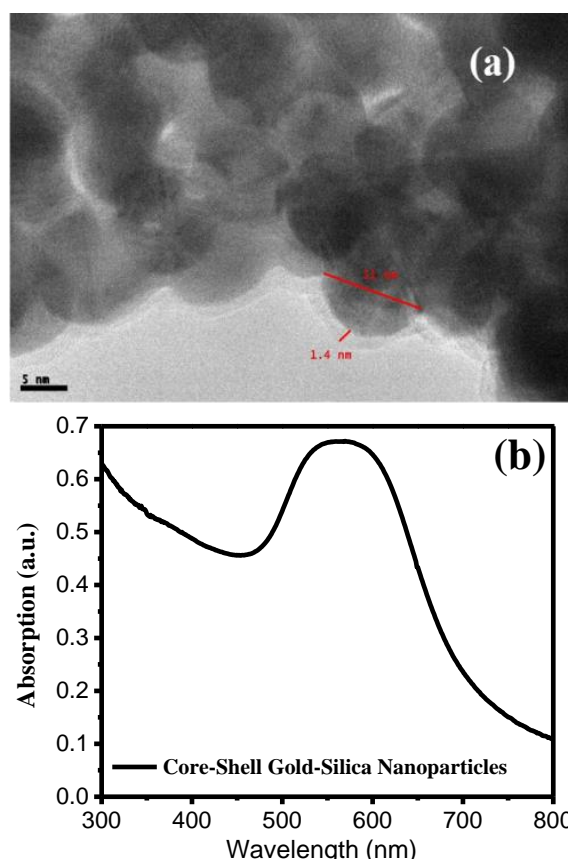

Fig. 2. (a) Transmission electron microscopy (TEM) image of core-shell Au@SiO$_2$ NPs, (b)

optical absorption spectrum of the core-shell sample in water.

Perovskite solar cells were fabricated on a structure based on Fluorine-doped Tin Oxide glass (FTO) glasses, which were partially etched using 2 M HCl and Zn powder, cleaned by the following procedure: cleaning with soap (Hellmanex) and deionized water, sonication in a mixture of acetone/ethanol (1:1 v/v) for 30 min, sonication in a mixture of acetone/isopropanol (1:1 v/v) for 30 min and drying with compressed air and then heating up to 80°C for 30 min. after that, UV-ozone treatment was performed for 15 min. To prepare the TiO_2 blocking layer (bl-TiO_2), titanium diisopropoxide dis(acetylacetonate) (Sigma-Aldrich, 75 wt% in isopropanol) in ethanol (1:9 v/v) was deposited by spray pyrolysis at 450° C with oxygen as carrier gas and then annealed at 450°C for 30 min in air. A Au sol is prepared based Turkevich procedures [17]. An average diameter of Au was around 11 nm. Au@SiO_2 core-shell NPs were prepared according to the synthetic protocol of Liz-Marzan [18]. The thickness of silica shell was about 1.4 nm. A thin layer of Au@SiO_2 was deposited by spin coating on the top and the bottom of the mp-TiO_2 layers and then annealed at 100 °C for 10 min. A diluted commercial TiO_2 paste (DSL 30NRT, Dyesol) in ethanol (1:5, weight ratio) was then deposited on the bl-TiO_2 by spin-coating at 2000 rpm for 10 seconds. After drying at 100° C for 10 min, annealed in air up to 500° C for 30 min. Lithium bis-(strifluoromethane sulfonamide) (LiTFSI) 35 mM solution in acetonitrile was deposited by spin coating onto the substrates at 3000 rpm for 10 seconds. Then the films were annealed at 450° C for 30 minutes [19]. 622 mg of PbI_2 (TCI, 99.999%), 214 mg of CH_3NH_3I (Dyesol), and 105 mg of DMSO (molar ratio 1:1:1) was mixed in 944 mg of DMF solution inside a glove box. The completely dissolved solution was spin-coated on the mp-TiO_2 layers at 4000 rpm for 50 seconds. Five seconds after rotation, diethyl ether was dripped on the rotating substrate before it becomes dark color due to the rapid vaporization of DMF [20]. After depositions, layers were heated at 100°C

for 3 min and a dense $CH_3NH_3PbI_3$ film was obtained. Then spiro-OMeTAD based HTL (72.3 mg spiro-OMeTAD, 28.8 μL 4-tert-butyl pyridine (tBP) and 17.5 μL Li-TFSI solution (520 mg/mL of Li-TFSI in acetonitrile) all dissolved in 1 mL chlorobenzene and then deposited on perovskite layer by spin-coating at 4000 rpm for 30 seconds. The cells were dried at 100° C for 3 min. Finally, the devices were transferred into a vacuum chamber for deposition of 60 nm Au by thermal evaporation in high vacuum system to form the electrode contacts.

B. *Characterization Methods*

The current-voltage curves were measured with a scan rate of 50 mV/s in Abet Technologies Sun 2000 Class A solar simulator with a Keithley 2612 Source Meter, AM1.5G where the light intensity was adjusted with an NREL-calibrated Si solar cell with a KG-5 filter to 1 sun of intensity (100 mW/cm^2). The measurements were performed using a shadow mask whose area was 0.101 cm^2. The morphology of the films was analyzed by scanning electron microscopy (SEM) using a JSM7001F (Field emission scanning electron microscope) and IPCE spectra were measured in air using a xenon lamp power source coupled with a monochromator controlled by a computer and optical power meter (Oriel Instruments, model 7310) and a Si photodiode to calibrate the system. UV-Visible absorption measurement was carried out using a double-beam spectrophotometer (JASCO, model 7800, Tokyo, Japan).

III. RESULTS AND DISCUSSION

Figure 3 displays a cross-sectional SEM image of FTO/ bl-TiO_2/ Au@SiO_2/ mp-TiO_2/ $CH_3NH_3PbI_3$/ Spiro/ Au. NPs were approximately spherical in shape. The thickness of bl is approximately 44 nm. The Au@SiO_2/ mp-TiO_2 layer is about 260 nm; and the $CH_3NH_3PbI_3$ perovskite was infiltrated into the pore of the mp-TiO_2 layer. A 270-nm-thick film of $CH_3NH_3PbI_3$ perovskite is clearly seen as the final layer. The thickness of spiro-

OMeTAD and Au is about 100 nm and 60 nm respectively.

As shown in Fig. 4, the absorption of Au@SiO$_2$ NPs was determined by UV–Vis spectrophotometry. A resonant peak in wavelengths around 659 nm is observed. The structure of FTO/ bl-TiO$_2$/ Au@SiO$_2$/ mp-TiO$_2$ layers have similar optical properties like the structure consisting FTO/ bl-TiO$_2$/ mp-TiO$_2$/ Au@SiO$_2$. No significant change is observed in the light absorption at the 500−650 nm wavelength region of compact/mp-TiO$_2$ layers with and without interfacial Au@SiO$_2$ NPs as shown in fig. 4. These observations rule out a direct plasmonic effect by an increase of light absorption in the solar cell enhancement observed when NPs are used at the interface.
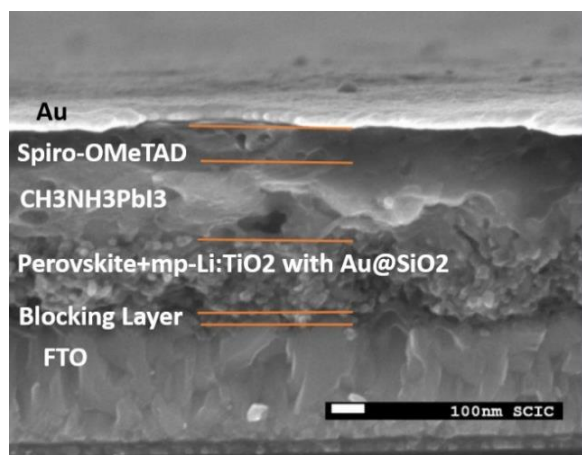

Fig. 3. The cross sectional SEM image of FTO/ bl-TiO$_2$/ Au@SiO$_2$/ mp-TiO$_2$/ CH$_3$NH$_3$PbI$_3$/ Spiro/ Au.
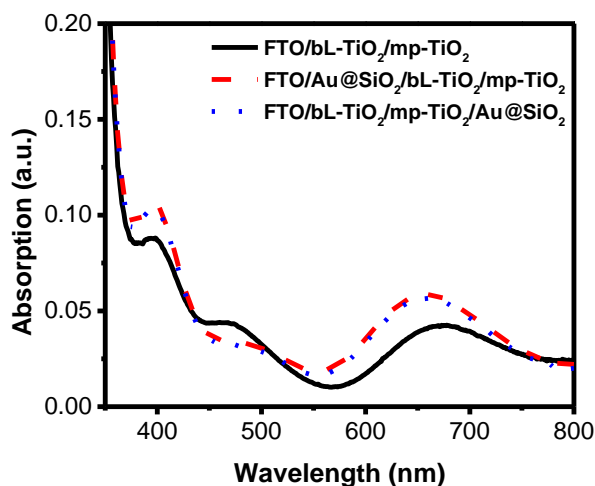

Fig. 4. Absorbance spectra of FTO/ bl- TiO$_2$/ Au@SiO$_2$/ mp-TiO$_2$/; FTO/ bl- TiO$_2$/ mp-TiO$_2$/ Au@SiO$_2$ and the reference cells.

The J-V curves of the references cells and modified cells with Au@SiO$_2$ NPs were measured under AM1.5 ((100 mW.cm^{-2})) in air (Fig. 5). The maximum power conversion efficiency (PCE) for the reference, FTO/ bl-TiO$_2$/ Au@SiO$_2$/ mp-TiO$_2$, and FTO/ bl-TiO$_2$/ mp-TiO$_2$/ Au@SiO$_2$ cells are 14.75, 17.55, and 15.00%, respectively. An Enhancement of 5% in short-circuit current density is observed for the cells consisting Au@SiO$_2$ bottom the mp-TiO$_2$ layers compared to the reference cells. The maximum J$_{sc}$ are 20.7 and 19.7 mA/cm^2, respectively. The J$_{sc}$ of cells consisting Au@SiO$_2$ top the mp-TiO$_2$ layer was almost close to the reference cells which suggests is due to the poor plasmonic effect due to the NPs size and position.
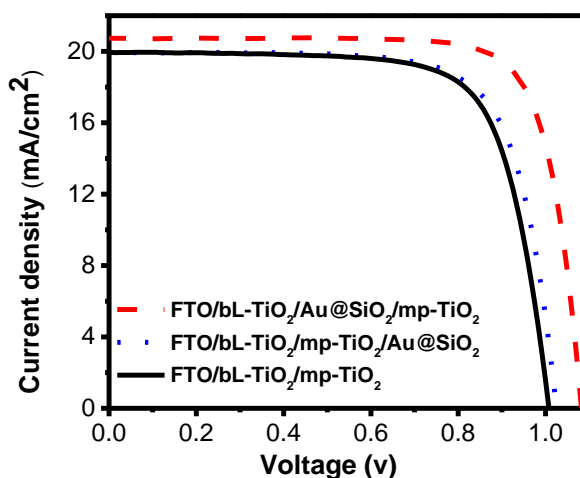

Fig. 5. The J–V curves of the cells consisting FTO/ bl- TiO$_2$/ Au@SiO$_2$/ mp-TiO$_2$/; FTO/ bl- TiO$_2$/ mp-

102

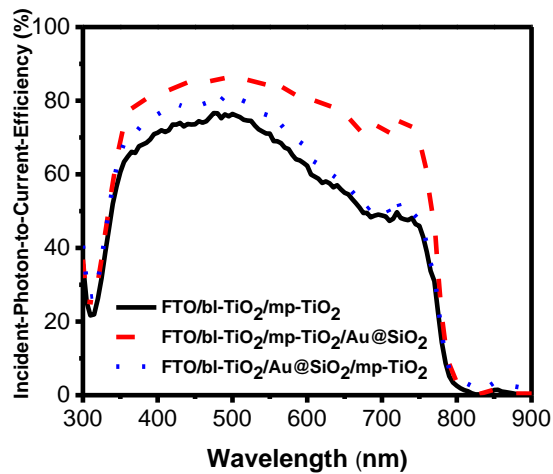TiO_2/ Au@SiO_2; and the refernce cells under AM1.5.

Fig. 6. The IPCE spectra the cells consisting FTO/ bl- TiO_2/ Au@SiO_2/ mp-TiO_2/; FTO/ bl- TiO_2/ mp-TiO_2/ Au@SiO_2; and the reference cells.

The J_{sc} value was consistent with that included from the incident-photon-to-current-efficiency (IPCE) spectra (Fig. 6). The Fig. 6 shows Au@SiO_2 NPs enhance charge separation. Modified cells with Au@SiO_2 NPs demonstrate an enhancement over the total wavelength range (300−800 nm) compared to the reference cells.

The results of reverse of the J–V measurements for 20 devices carried out at 1 sun illumination intensity are presented in

Table 1. From Table 1, we observed that the average J-V scanned PCE enhancement for the FTO/ bl-TiO_2/ Au@SiO_2/ mp-TiO_2 compared to FTO/ bl-TiO_2/ mp-TiO_2/ Au@SiO_2 and the reference cells, mainly comes from the greatly improved short-circuit photocurrent density (Jsc) and the open-circuit voltage (V_{oc}), while fill factor (FF) are only slightly changed. Figure 7 shows the average device performance parameters of cells with dissimilar place of Au@SiO_2 NPs as well as the reference cells. To ensure reliability of the measurements, at least 20 samples were fabricated for each model. The FF value is affected by both the shunt resistance and the series resistance of the devices. Therefore, the low fill factor may be resulted from a low shunt resistance and a high serial resistance, as shown in Table 1. The shunt resistance is lower for the reference samples, from the higher slope of the current density-potential (J−V) curve near 0 V as we can see in Fig. 5, and it results in lower solar cell performance. The low series resistance is observed in cells with Au@SiO_2 bottom of mp-TiO_2 as shown in Fig. 8. The lowest series resistance, indicating that addition of Au NPs can increase conductivity by improving mobility charge-transporters properties [8]. Interestingly, the main impact of a rising series resistance is to reduce FF, although series resistance does not affect Voc.

Table 1. Summary of efficiency of devices discussed in this work in the reverse.

	J_{sc} (mA/cm^2)	V_{oc} (mV)	FF (%)	PCE (%)	R_{shunt} (Ω. cm^2)	R_{series} (mΩ. cm^2)
FTO/bl-TiO_2/mp-TiO_2	19.1±0.5	973±30	69±2	13.6±1.3	$1.8\times10^5\pm4.1\times10^5$	2868±601
FTO/bl- TiO_2/ Au@SiO_2/mp-TiO_2	20.3±0.5	1007±43	73±4	15.8±1.7	$4.4\times10^7\pm4.9\times10^7$	2560±1637
FTO/bl-TiO_2/mp-TiO_2/Au@SiO_2	19.2±1.2	966±29	69±2	13.0±1.3	$2.3\times10^7\pm4.2\times10^7$	3291±730

Figure 9 depicts the electrochemical impedance spectra (EIS) and the corresponding Nyquist plots for PSCs. A Nyquist plot of impedance, $Z=Z'+Z''$, in which Z' is plotted in terms of Z'' presenting two semicircles each of which is related to an internal interface between two different

semiconductors [21]. EIS in Fig. 9 have been fitted using the equivalent circuit plotted in Fig. 10 [22]. Thereupon, the electrical behavior of the device was studied based on the equivalent circuit. In the EIS analysis, a DC potential bias was applied and overlapped

by a sinusoidal ac potential perturbation of 25 mV over a frequency range of 0.1 Hz-1 MHz.

Fig. 9 show the Nyquist plots of PSCs with Au@SiO₂ NPs, and the reference device without NPs, which showed rather higher efficiency than that of other devices. In the equivalent circuit, a series resistor R_S is the nonzero intercept on the real axis of the impedance plot, which denotes the sheet resistance of FTO and the contact resistance of FTO/TiO₂.

The first semicircle, which is related to a high-frequency arc, is associated with the diffusion of holes through the perovskite/Au counter electrode interface, which is modeled by an R_{CE} resistance. The arc was related to the recombination resistance, R_{rec}, in lower the frequency response, mainly due to the electron-hole recombination of at the mp-TiO₂/ CH₃NH₃PbI₃ interface.
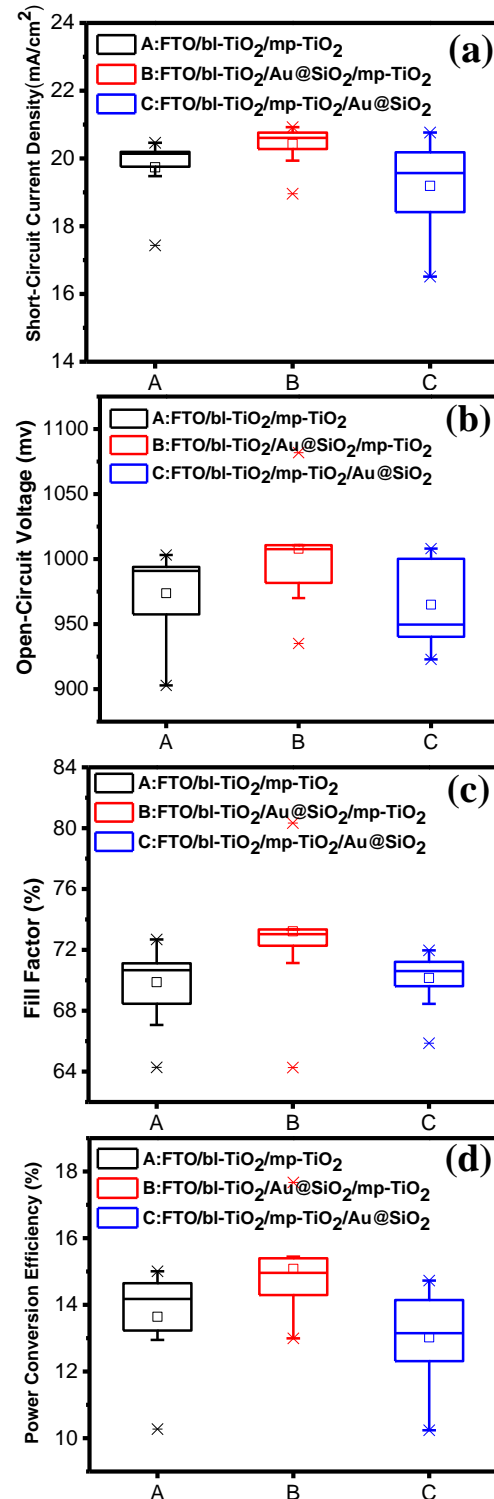

Fig. 7. Statistics parameters for the photovoltaic performance for 20 cells using different concentration of Au@SiO₂ (a) J_{SC}, (b) V_{OC}, (c) FF, (d) PCE. A:FTO/bl-TiO₂/mp-TiO₂, B:FTO/bl-TiO₂/Au@SiO₂/ mp- TiO₂, C:FTO/bl-TiO₂/mp-TiO₂/Au@SiO₂.

The resistance for the entire device with the Au@SiO₂ NPs was smaller than that of the reference device due to the presence of Au@SiO₂ NPs. As compared to the reference

104

device, the diameter of semicircles R_{rec} clearly decreased after doping NPs on the top and the bottom of the mp-TiO_2 layer. Thus, it is suggested that Au@SiO_2 NPs in the device can improve not only the optical properties but also the electrical properties [21]. In the compare two position of deposition Au@SiO_2 NPs, it is apparent that Rrec decreased after deposition Au@SiO_2 NPs on the bottom position of mp-TiO_2.
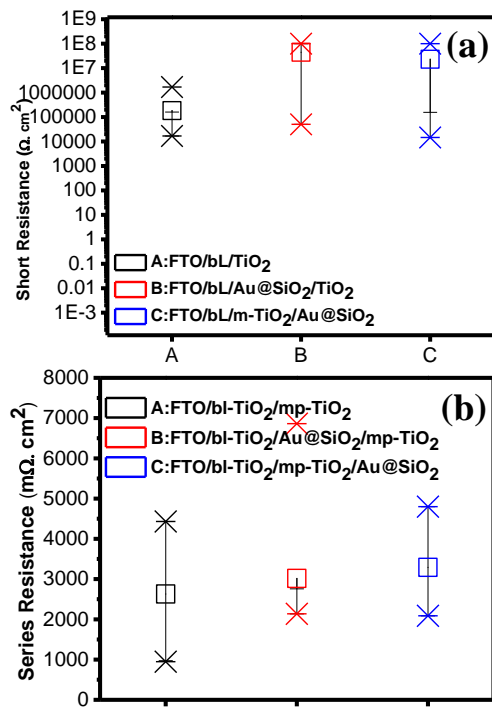

Fig. 8. (a) R_{sh} (shunt resistance), (b) R_s (series resistance). A:FTO/bl-TiO_2/mp-TiO_2,B:FTO/bl-TiO_2/Au@SiO_2/mp- TiO_2, C:FTO/bl-TiO_2/mp-TiO_2/Au@SiO_2.
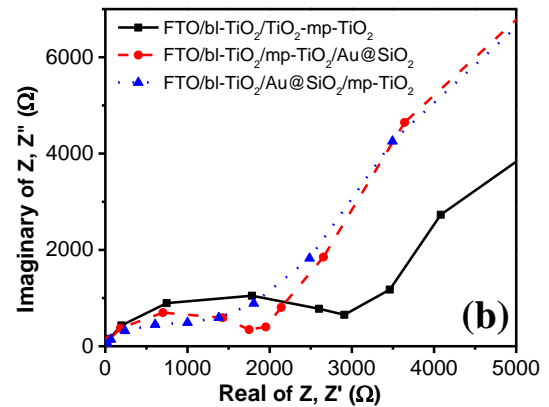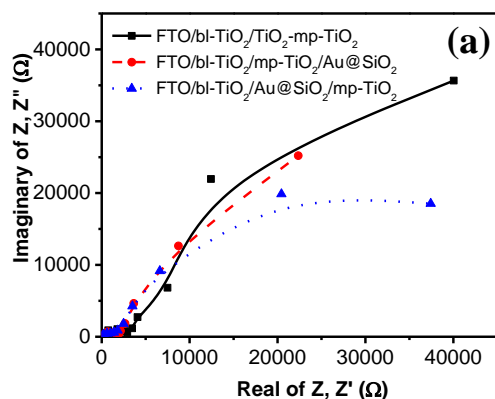

Fig. 9. The EIS using 0.2 V as applied DC voltage for sample without NP (FTO/bl-TiO_2/ mp-TiO_2) and with difference deposition place NPs (FTO/bl-TiO_2/Au@SiO_2/mp-TiO_2 and FTO/bl-TiO_2/ mp-TiO_2/Au@SiO_2) (a) complete spectra; (b) zoom of different region of the complete plot.
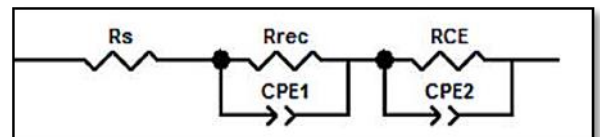

Fig. 10 Equivalent circuit model employed for impedance analysis of the perovskite solar cells

IV. CONCLUSION

In conclusion, we have synthesized Au@SiO_2 NP. They were then deposited bottom and top of mesoporous TiO_2 layer. The effect of using these NPs on the performance of the fabricated cells were studied. Although we expected an increase in J_{SC}; V_{OC}, and FF for both structures, the cells with FTO/ bl-TiO_2/ Au@SiO_2/ mp-TiO_2 structure showed significant enhancement in photocurrent response compared to the reference cells. Although both cells consisting FTO/ bl-TiO_2/ Au@SiO_2/ mp-TiO_2 and FTO/ bl-TiO_2/ mp-TiO_2/ Au@SiO_2 structures show similar absorption in the visible region. However, fabricated cells have different photovoltaic properties. The FTO/ bl-TiO_2/Au@SiO_2/ mp-TiO_2 cells also demonstrate improved IPCE compared to the reference cell, suggesting suitable surface engineering of the structure with an enhancement over the total wavelength visible range compared to the reference cells.

REFERENCES

[1] S. Aharon, B. El Cohen, and L. Etgar, "Hybrid Lead Halide Iodide and Lead Halide Bromide in Efficient Hole Conductor Free Perovskite Solar Cell," J. Phys. Chem. C, vol. 118, pp. 17160–17165, 2014.

[2] A. Kojima, K. Teshima, Y. Shirai, and T. Miyasaka, "Organometal halide perovskites as visible-light sensitizers for photovoltaic cells," J. Am. Chem. Soc., vol. 131, pp. 6050–6051, 2009.

[3] "National Renewable Energy Laboratory, Best Research-Cell Efficiencies chart, http://www.nrel.gov/ncpv/images/efficiency_chart.jpg, Accessed 13.03," 2016.

[4] M. K. Gangishetty, K. E. Lee, R. W. J. Scott, and T. L. Kelly, "Plasmonic Enhancement of Dye Sensitized Solar Cells in the Red-to-near-Infrared Region using Triangular Core Shell Ag@SiO₂ Nanoparticles," ACS Appl. Mater. Interfaces, vol. 5, pp. 11044–11051, 2013.

[5] F. Huang, D. Chen, X. L. Zhang, R. A. Caruso, and Y.-B. Cheng, "Dual-Function Scattering Layer of Submicrometer-Sized Mesoporous TiO₂ Beads for High-Efficiency Dye-Sensitized Solar Cells," Adv. Funct. Mater., vol. 20, pp. 1301–1305, 2010.

[6] P. Balrajua, P. Suresha, M. Kumarb, M. S. Royb, and G. D. Sharma, "Effect of counter electrode, thickness and sintering temperature of TiO₂ electrode and TBP addition in electrolyte on photovoltaic performance of dye sensitized solar cell using pyronine G (PYR) dye," J. Photochem. Photobiol. A Chem., vol. 206, pp. 53–63, 2009.

[7] G. Kakavelakis, K. Alexaki, E. Stratakis, and E. Kymakis, "Efficiency and stability enhancement of inverted perovskite solar cells via the addition of metal nanoparticles in the hole transport layer," RSC Adv., vol. 7, pp. 12998–13002, 2017.

[8] C. Zhang, Q. Luo, J. Shi, L. Yue, Z. Wang, X. Chen, and S. Huang, "Efficient Perovskite Solar Cells by Combination use of Au Nanoparticles and Insulating Metal Oxide," Nanoscale, vol. 9, pp. 2852–2864, 2017.

[9] T. Ye, S. Ma, X. Jiang, L. Wei, C. Vijila, and S. Ramakrishna, "Performance Enhancement of Tri-Cation and Dual-Anion Mixed Perovskite Solar Cells by Au@SiO₂ Nanoparticles," Adv. Funct. Mater, vol. 27, pp. 1606545 (1-9), 2017.

[10] W. Zhang, M. Saliba, S. D. Stranks, Y. Sun, X. Shi, U. Wiesner, and H. J. Snaith, "repeat-Enhancement of perovskite-based solar cells employing core-shell metal nanoparticles.," Nano Lett., vol. 13, pp. 4505–10, 2013.

[11] M. Saliba, W. Zhang, V. M. Burlakov, S. D. Stranks, Y. Sun, J. M. Ball, M. B. Johnston, A. Goriely, U. Wiesner, and H. J. Snaith, "Plasmonic-Induced Photon Recycling in Metal Halide Perovskite Solar Cells," Adv. Funct. Mater., vol. 25, pp. 5038–5046, 2015.

[12] Z. Lu, X. Pan, Y. Ma, Y. Li, L. Zheng, D. Zhang, Q. Xu, Z. Chen, S. Wang, B. Qu, F. Liu, Y. Huang, L. Xiao, and Q. Gong, "Plasmonic-Enhanced Perovskite Solar Cells Using Alloy Popcorn Nanoparticles," RSC Adv., vol. 5, pp. 11175–11179, 2015.

[13] N. K. Pathak, N. Chander, V. K. Komarala, and R. P. Sharma, "Plasmonic Perovskite Solar Cells Utilizing Au@SiO₂ Core-Shell Nanoparticles," Plasmonics, pp. 1–8, 2016.

[14] E. S. Arinze, B. Qiu, G. Nyirjesy, and S. M. Thon, "Plasmonic Nanoparticle Enhancement of Solution- Processed Solar Cells: Practical Limits and Opportunities," ACS Photonics, vol. 3, pp. 158–173, 2016.

[15] H. Nourolahi, A. Behjat, S. M. M. H. Zarch, and M. A. Bolorizadeh, "Silver nanoparticle plasmonic effects on hole-transport material-free mesoporous heterojunction perovskite solar cells," Sol. Energy, vol. 139, pp. 475–483, 2016.

[16] N. Aeineh, E. M. Barea, A. Behjat, N. Sharifi, and I. Mora-Sero, "Inorganic Surface Engineering to Enhance Perovskite Solar Cell Efficiency," ACS Appl. Mater. Interfaces, vol. 9, pp. 13181–13187, 2017.

[17] B. V. Enustun and J. Turkevich, "Coagulation of Colloidal Gold," J. Am. Chem. Soc., vol. 85, pp. 3317–3328, 1963.

[18] L. M. Liz-marza, M. Giersig, and P. Mulvaney, "Synthesis of Nanosized Gold - Silica Core - Shell Particles," Langmuir, vol. 12, pp. 4329–4335, 1996.

[19] F. Giordano, A. Abate, J. P. C. Baena, M. Saliba, T. Matsui, S. H. Im, S. M. Zakeeruddin, M. K. Nazeeruddin, A. Hagfeldt, and M. Graetzel, "Enhanced electronic properties in mesoporous TiO_2 via lithium doping for high-efficiency perovskite solar cells," Nat. Commun., vol. 7, pp. 10379-10384, 2016.

[20] N. Ahn, D.-Y. Son, I.-H. Jang, S. M. Kang, M. Choi, and N.-G. Park, "Highly Reproducible Perovskite Solar Cells with Average Efficiency of 18.3% and Best Efficiency of 19.7% Fabricated via Lewis Base Adduct of Lead(II) Iodide," J. Am. Chem. Soc., vol. 137, pp. 8696–8699, 2015.

[21] A. Todinova, J. Idígoras, M. Salado, S. Kazim, and J. A. Anta, "Universal Features of Electron Dynamics in Solar Cells with TiO_2 Contact: From Dye Solar Cells to Perovskite Solar Cells," J. Phys. Chem. Lett., vol. 6, pp. 3923–3930, 2015.

[22] J. Bisquert and V. S. Vikhrenko, "Interpretation of the Time Constants Measured by Kinetic Techniques in nanostructured semiconductor electrodes and dye-sensitized solar cells," J. Phys. Chem. B, vol. 108, pp. 2313–2322, 2004.

Naemeh Aeineh received her M.Sc. degree in Atomic and Molecular Physics from Iran University of Science and Technology (IUST), Iran in 2009. She is pursuing her study towards Ph.D. in Atomic and Molecular Physics at Yazd University under the supervision of Prof. Behjat. Her research focuses on the interactions of nanoparticles with third generation solar cell materials including Organic semiconductors and perovskites solar cells.

Dr. Abbas Behjat is the Professor of Physics, at Yazd University, Iran. He obtained his Ph.D. in x-ray lasers from the Essex University, England in 1996. Currently, he is group leader in the Photonics Research Group (PRG), Engineering Research Center, at Yazd University. Since 2007, he has been mainly involved in nanostructure-based optical devices including light emitting diodes, quantum dots and dye sensitized solar cells and perovskite and also polymer bulk heterojunction solar cells.

Nafiseh Sharifi received her B.Sc. and M.Sc. degrees in physics from Alzahra University and Sharif University of Technology (SUT), Tehran, Iran, respectively. She obtained her Ph.D. in nanotechnology under the supervision of Dr. Taghavinia, from Sharif University of Technology in 2012. She was a postdoctoral researcher at Sharif University of Technology until 2013 when she became an Assistant Professor at the University of Kashan. Her research interests include optoelectronic devices, dye-sensitized solar cells, provskite solar cells, plasmonics and electrochemical sensors.

THIS PAGE IS INTENTIONALLY LEFT BLANK.